THE ROLE OF THE EARLY DIAGENETIC DOLOMITIC CONCRETIONS IN THE PRESERVATION OF THE 2.1 GA PAEOLENVIRONMENTAL SIGNAL: PALEOPROTEROZOIC OF THE FRANCEVILLE BASIN, GABON

Nathaelle ONANGA MAVOTCHY, Abderrazak EL ALBANI*, Alain TRENTESAUX, Claude FONTAINE, Anne-Catherine PIERSON-WICKMANN, Philippe BOULVAIS, Armelle RIBOULLEAU, Lauriss NGOMBI PEMBA, Florent PAMBO, François GAUTHIER-LAFAYE

*Corresponding author

Supplementary material

Supplementary information

1- Geological setting

The FA Formation is essentially formed of fluvial and deltaic sandstone deposits on top of which are located the well-known Oklo nuclear reactors (Gauthier-Lafaye and Weber, 1989; 2003; Gauthier-Lafaye et al., 1989). A transition from siliciclastic-dominated fluvial-deltaic to marine sedimentation is systematically observed at the top of the FA Formation (Gauthier-Lafaye and Weber 2003; Préat et al., 2011).

The FB unit consists of marine sediments deposited mainly below storm wave base. Because of its diverse lithological composition, the FB unit is further divided into the FB1 (a, b, and c) and FB2 (a and b) subunits. The FB1a and FB1b subunits consist of interlayered shales, sandstones, and conglomerates, fining upwards to predominantly shales at the top. The FB1c subunit mainly consists of shales, but also contains a thin iron formation overlain by black shales and a thick interval rich in manganese (Mn). The FB2a subunit consists of sandstone beds deposited in channels near the fair-weather wave base. These are sharply overlain by the FB2b subunit including finely-laminated black shales interbedded with thin siltstone layers deposited by waning storm surges. The previously reported large colonial organisms (El Albani et al., 2010, 2014), were collected from the FB2b black shales.

The overlying FC Unit is dominated by dolomites and stromatolitic cherts, indicating shallow-water conditions. Stromatolites are found on topographic highs at the base of the FC unit (Weber, 1968). The FD unit corresponds to black shales deposited during a transgressive phase (Canfield et al., 2013, Ngombi-Pemba et al., 2014).

2-Materials and methods

Carbonate concretion samples were collected in the Moanda area. From polished sections, the concretions and surrounding black shales were characterised by optical microscopy and scanning electron microscopy (SEM). After carbon metallization, the samples were observed using the FEI Quanta 200 microscope from the UMR 8187 LOG CNRS-University of Lille, which is equipped with an EDS system and uses a Bruker Xflash 3001 detector associated to a Quantax software. Analytical conditions were an accelerating voltage of 15 kV and a working distance of 10 mm in backscattered or secondary electron mode. The global mineralogical composition of these samples was determined by X-ray diffraction (XRD) using the ANAlytical XpertPro diffractometer from the UMR 7285 IC2MP CNRS-University of Poitiers. Major, minor, trace and rare earth elements in bulk sediment were analyzed at the Service d'Analyse des Roches et des Minéraux facility of the Centre National de la Recherche Scientifique (Vandœuvre-les-Nancy, France) using ICP-AES (major and minor elements) and ICP-MS (trace and rare earth elements) after fusion with $LiBO_2$ and HNO_3 dissolution. Precision and accuracy were better than 1% (mean 0.5%) for major and minor elements and better than 5% for trace and rare earth elements, as checked by international standards and analysis of replicate samples (Carignan et al., 2001). Analyses of stable isotopes ($\delta^{13}C$, $\delta^{18}O$) were performed on 27 host rock and carbonate concretion samples. Carbonates were reacted with anhydrous phosphoric acid under thermostated conditions (50°C) until completion. The isotopic compositions were measured on a VG Optima triple collector mass spectrometer at the stable isotope laboratory from the UMR 6118 Géosciences Rennes CNRS-University of Rennes 1. The isotopic ratios are expressed in ‰ relative to the PDB

(*Belemnitella americana* of Pee Dee Formation). The analytical uncertainty is ±0.2‰ for O, and ±0.1‰ for C; it was estimated using replicate analysis of some samples and reproducibility of international (NBS 19) and in-house (Prolabo Rennes) standarts. Samples for organic carbon analysis were treated with 10% HCl to remove carbonate, rinsed with distilled water, and freeze-dried. The isotopic composition of organic carbon was then determined using an elemental analyzer (EA-CE 1500 NA, Carlo Erba) coupled with an isotope ratio mass spectrometer (IRMS) (VG Isoprime; UMR PEGASE – INRA Rennes). Tin capsules were used for sample loading. The analytical uncertainty is ±0.2‰ for C of organic carbon.

Supplementary figures

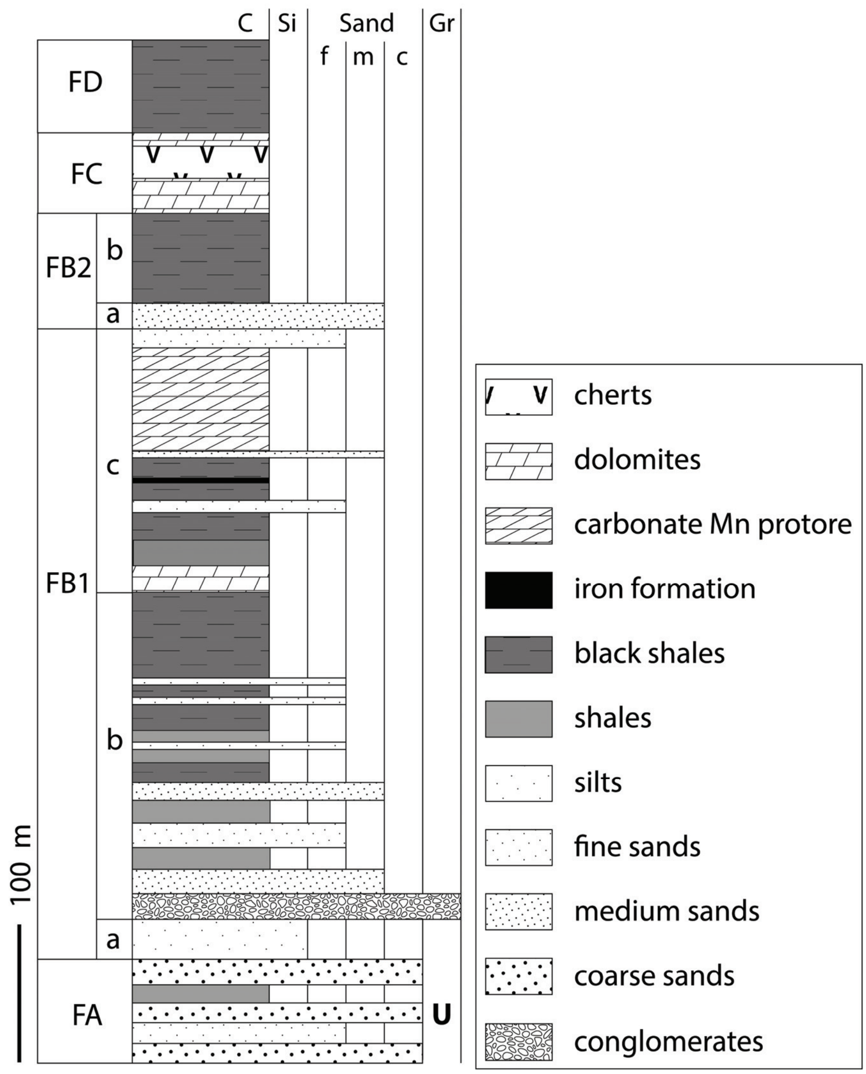

Figure S1: Lithostratigraphic column of the Francevillian Group.

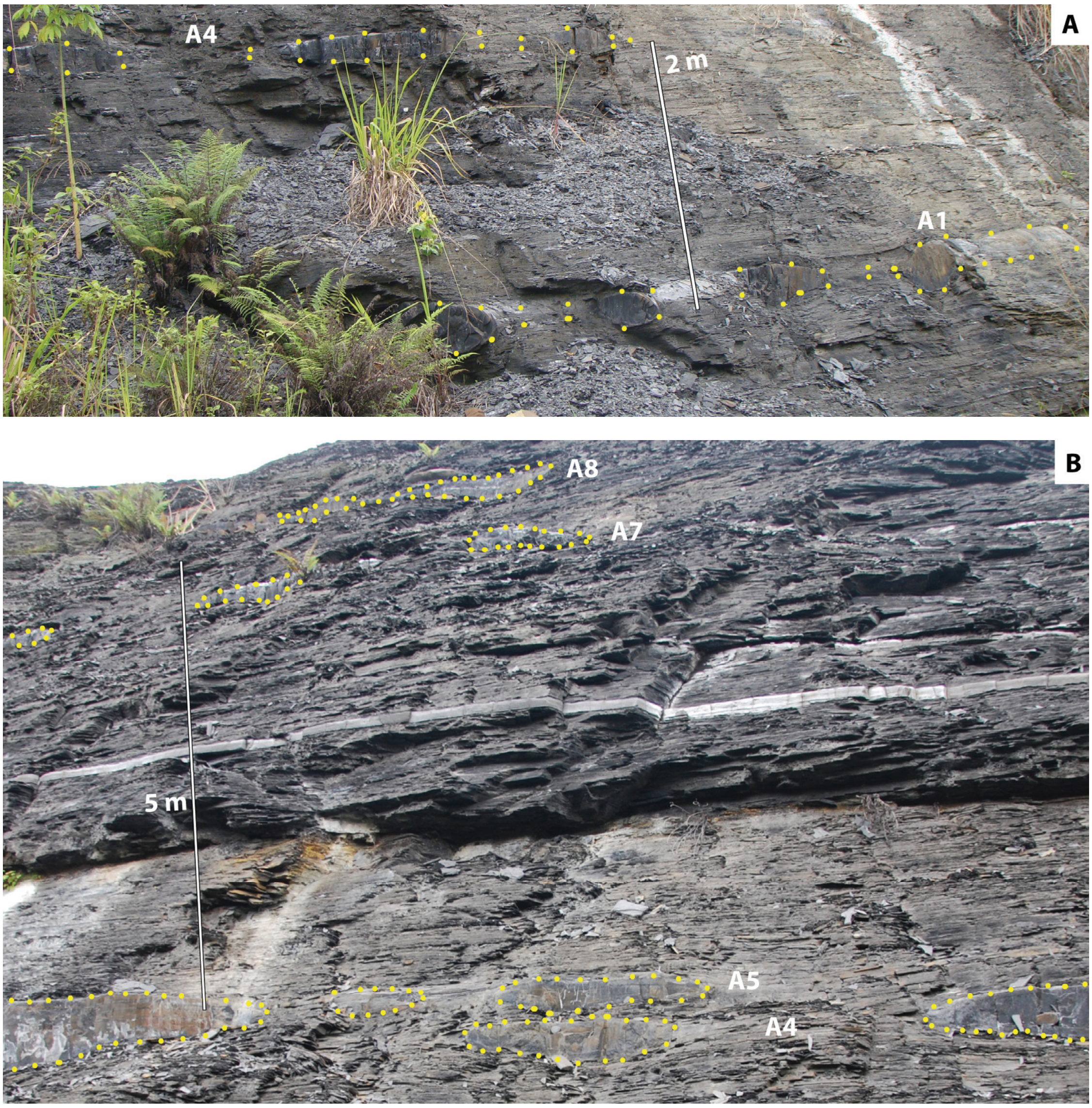

Figure S2: Distribution of carbonate concretions and silt-sandstone beds within host black-shales (yellow dots) in the Francevillian B Formation at the Moanda station. (A) Lower section displaying alignments A1 and A4. (B) Upper section displaying alignments A4 to A8. The middle grey layer corresponds to a fine sandstone layer (see **Fig. 2**). Note that some alignments are not visible at this scale.

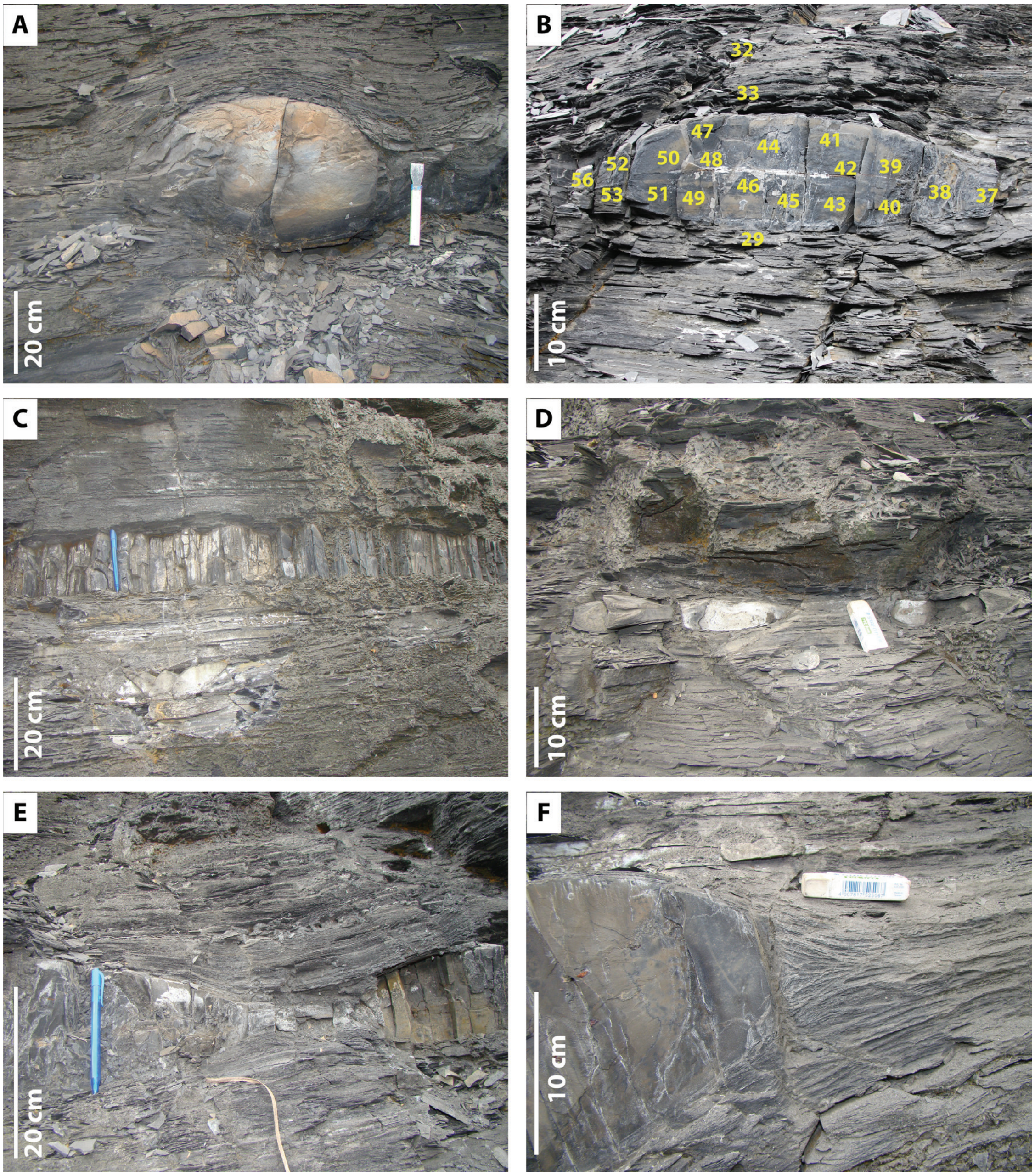

Figure S3: Morphologies of carbonate concretions within the black shale host in the Francevillian B formation. (A) Rounded concretion, (B) Ellipsoidal (flattened) concretion (alignment A5, nodule N1). Numbers refer to analyzed samples, (C) Flattened and fractured concretions of more than 2-m long, (D) Ellipsoidal concretions of 5 to 15 cm long, (E and C) differential compaction of black shale host around concretions.

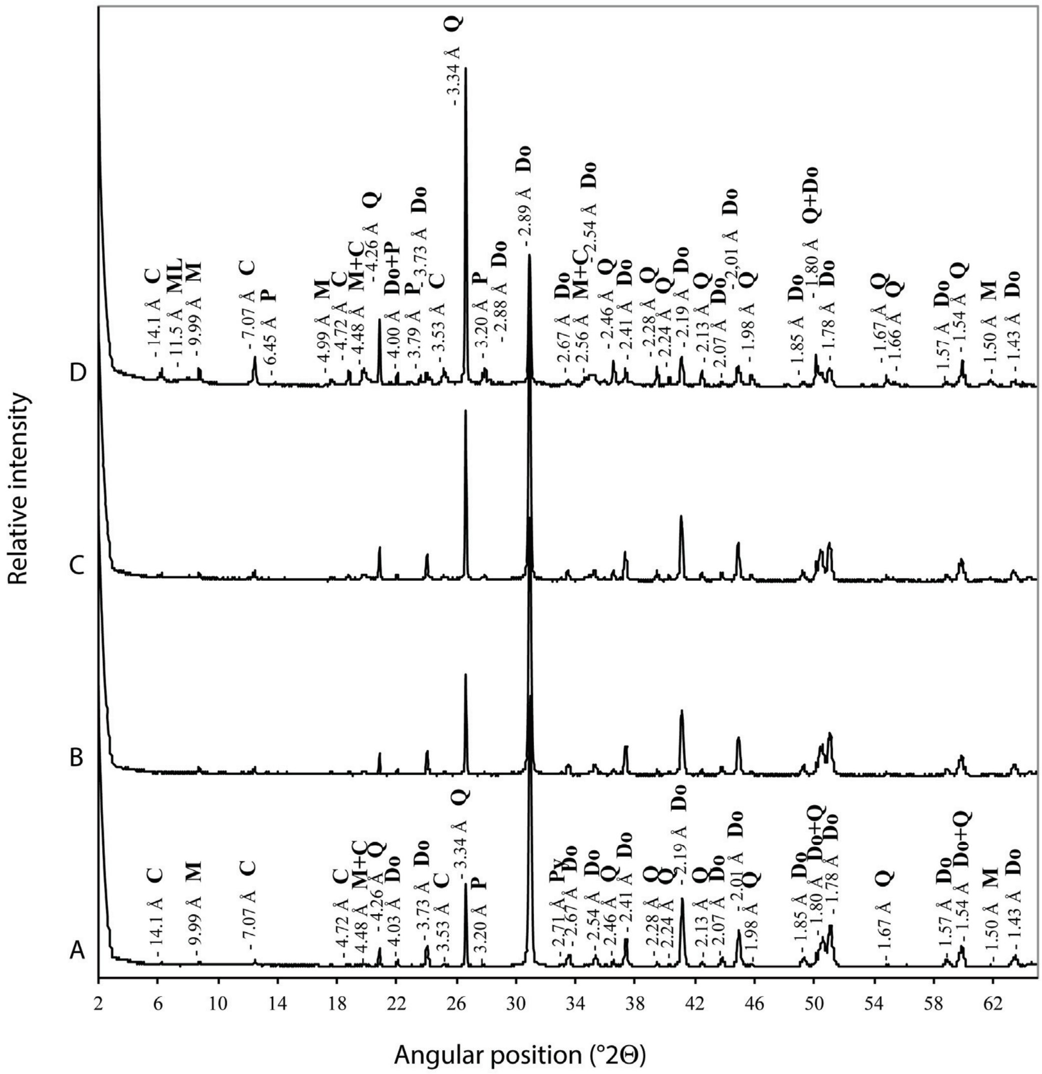

Figure S4: XRD Powder diffractograms of different samples from the centre of a concretion (A) to the upper and lower edges (B) and lateral edge (C), and in the black shale host rock (D). Identified minerals are Dolomite (Do), Pyrite (Py), Quartz (Q), Plagioclase (P), Mica or Illite (M), Chlorite (C), and Mixed-layer (ML).

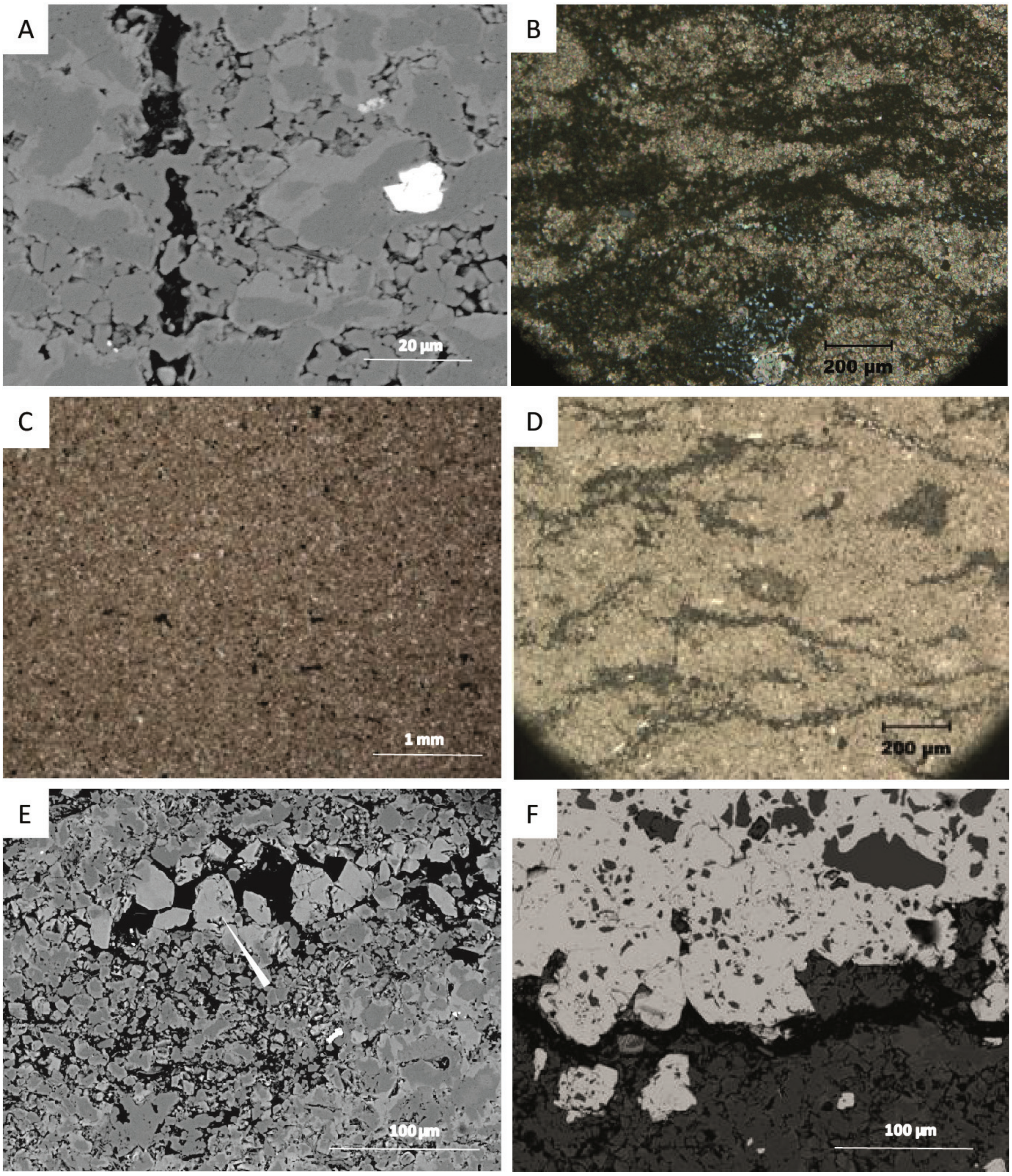

Figure S5: Petrography of internal structure of ovoid concretion in alignment A5: (A) Dolomitic matrix showing two dolomitic phases (Ferroan dolomite (clear) and pure dolomite (dark) in the part of the concretions; (B) view of an organic-rich lamina showing wavy lamination; (C) close to the central pyritic stripe, small organic matter clusters in an homogenous matrix; (D) at the top of concretion, disperse patches of organic matter; (E) recrystallised dolomite in the porosity (arrow) close to the host-rock.

(F) Massive pyrite crystals (light grey) in the centre of each concretion and enclosing xenomorphic dolomite (dark grey).

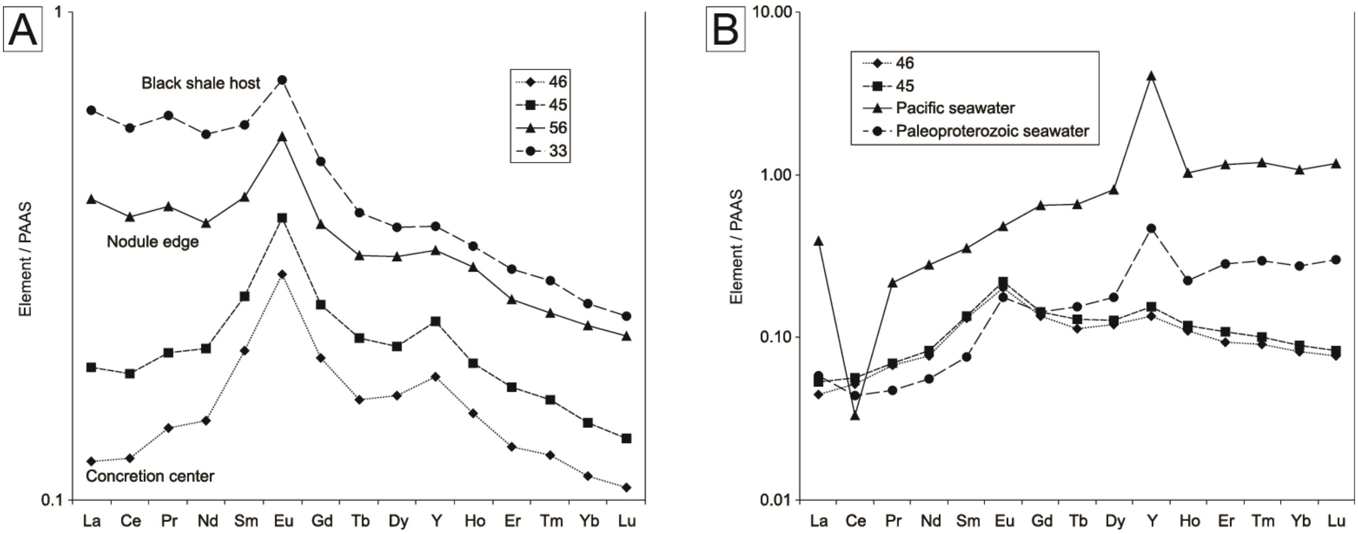

Figure S6: (A) PAAS-normalised REE+Y patterns of carbonate concretion (center #45, #46; see **Suppl. Tab. 2**) and edge (#56)), and black shale host rock (#33). (B) PAAS normalised REE+Y pattern of the carbonate phase in the nodule centre (#45, #46) compared to present day Pacific seawater (Alibo and Nozaki, 1999) and Paleoproterozoic seawater (Bau and Dulski, 1996). PAAS values according to Taylor and MacLennan (1985).

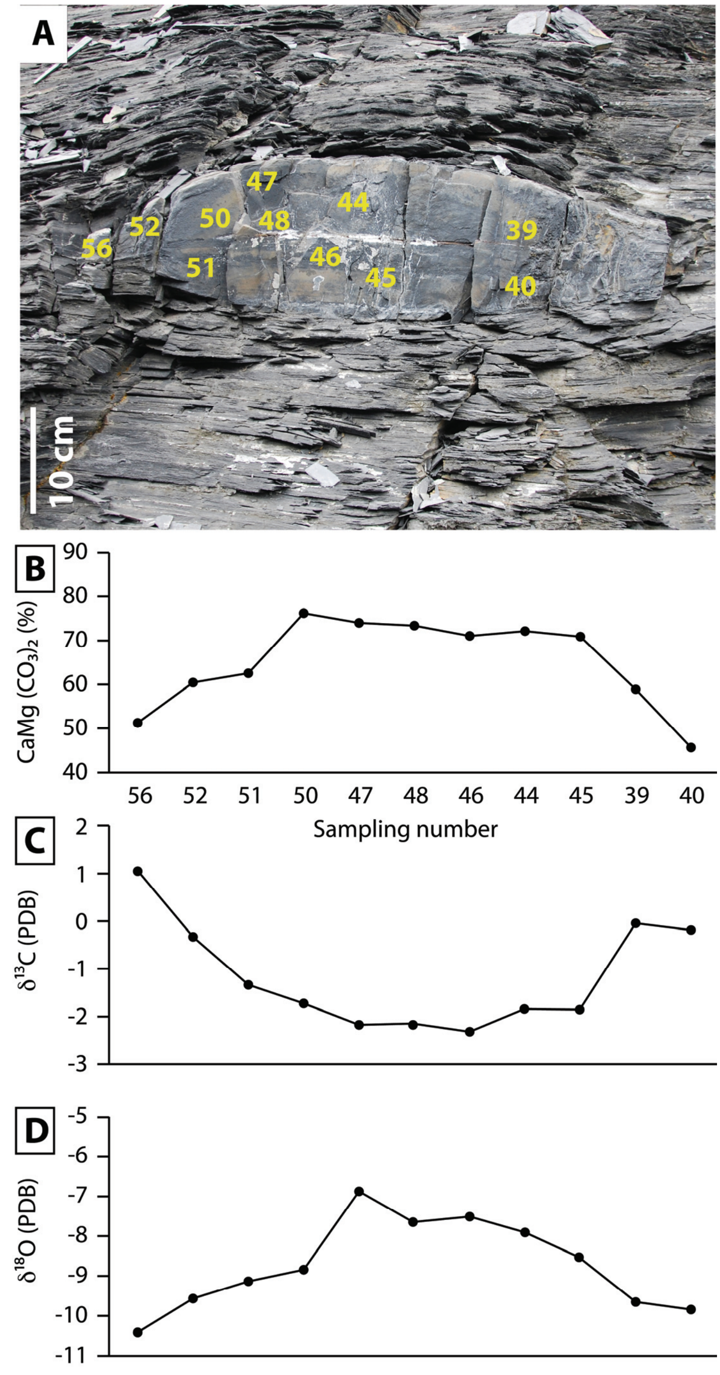

Figure S7: Lateral evolution in dolomitic concretion (A) of the carbonate content $CaMg(CO_3)_2$, (B), the carbon (C), and the oxygen (D) isotope compositions of the carbonate fraction.

Supplementary tables

Supplementary table 1: Evolution of cristallographic parameters of reflection (104) of dolomites in the different concretions in alignments A1, A4, A5, A7 and A8 (**Figs. 2, S2**).

Concretion alignment	**Sample #**	**Dolomite-Fe**				**Dolomite**				**DoFe/Do**
		d(104) (Å)	Position (°2θ)	FWHM (°2θ)	Area cts. °2θ	d(104) (Å)	Position 2θ	FWHM 2θ	Area cts. 2θ	area/area
A8	77	0.00	0.00	0.00	0.00	2.88	30.99	0.21	1471	0.00
A7	72	0.00	0.00	0.00	0.00	2.89	30.96	0.15	992	0.00
A5	51	2.89	30.89	0.12	1903	2.89	30.97	0.07	503	3.78
A5	50	2.89	30.89	0.13	1809	2.89	30.97	0.07	608	2.98
A5	48	2.89	30.88	0.11	1450	2.88	30.98	0.10	1469	0.99
A5	47	2.89	30.87	0.09	608	2.88	30.98	0.13	2119	0.29
A5	46	2.89	30.87	0.10	846	2.89	30.97	0.13	1844	0.46
A5	45	2.89	30.87	0.11	1204	2.89	30.97	0.12	1445	0.83
A5	44	2.89	30.89	0.11	1317	2.88	30.97	0.11	1508	0.87
A5	43	2.89	30.89	0.12	1545	2.89	30.97	0.08	661	2.34
A5	42	2.89	30.90	0.13	1539	2.88	30.97	0.08	729	2.11
A5	41	2.89	30.90	0.14	1698	2.88	30.98	0.08	501	3.39
A4	16	2.89	30.84	0.16	346	2.88	30.99	0.18	765	0.45
A1	3	2.90	30.80	0.16	174	2.88	3.097	0.25	786	0.22

Supplementary table 2: Geochemical data on the Paleoproterozoic concretions and enclosing rock in Moanda section. See accompanying .xls file

Supplementary table 3: Paleotemperature calculated from the oxygen isotope composition of the centre of Moanda concretions, using different seawater-dolomite fractionation factors, and using different values for the isotopic composition of seawater ($\delta^{18}O_w$): value for an ice-free world (-1‰) and different values for Paleoproterozoic seawater (-8.5 and -6‰; Jaffrés et al. 2007). The temperature dependence of the fractionation factor α is calculated using the equation: $10^3 \ln \alpha = A.10^6 / T^2 + B.10^3 / T + C$

	Vasconcelos et al. (2005)	Matthews et al. (1977)	Fritz and Smith (1970)	Zheng (1999)
Parameters for the equation				
A	2.73	3.06	2.62	4.06
B	0	0	0	-4.65
C	0.26	-3.24	2.1	1.71
Calculated paleotemperature (°C)				
Nodule 1, $\delta^{18}O$ = -7.6 ‰ (PDB)				
$\delta^{18}O_w$ = -1 ‰ (SMOW)	67.4	63.3	74.7	63.1
$\delta^{18}O_w$ = -8.5 ‰ (SMOW)	23.3	24.4	26.6	26.9
$\delta^{18}O_w$ = -6 ‰ (SMOW)	36.1	35.9	40.3	37.6
Nodule 2, $\delta^{18}O$ = -7.9 ‰ (PDB)				
$\delta^{18}O_w$ = -1 ‰ (SMOW)	69.6	65.2	77.1	64.9
$\delta^{18}O_w$ = -8.5 ‰ (SMOW)	24.8	25.7	28.1	28.1
$\delta^{18}O_w$ = -6 ‰ (SMOW)	37.7	37.3	42.1	38.9

References

Alibo, D.S., Nozaki, Y., 1999. Rare earth elements in seawater: Particle association, shale-normalization and Ce oxidation. Geochim. Cosmochim. Acta 63, 363–372.

Bau, M., Dulski, P., 1996. Distribution of yttrium and rare-earth elements in the Penge and Kuruman iron-formations, Transvaal Supergroup, South Africa. Precam. Res. 79, 37-55.

Canfield, D.E., Ngombi-Pemba, L., Hammarund, E.U., Bengston, S., Chaussidon, M., Gauthier-Lafaye, F., Meunier, A., Riboulleau, A., Rollion-Bard, C., Rouxel, O., Asael, D., Pierson-Wickmann, A.-C., El Albani, A., 2013. Oxygen dynamics in the aftermath of the Great Oxidation of Earth’s atmosphere. PNAS 110, 16736-16741.

Carignan, J., Hild, P., Mevelle, G., Morel, J., Yeghicheyan, D., 2001. Routine analyses of trace elements in geological samples using flow injection and low pressure on-line liquid chromatography coupled to ICP-MS: A study of geochemical reference materials BR, DR-N, UB-N, AN-G and GH. Geostandard Newslett. 25, 187-198.

El Albani, A., Bengton, S., Canfield, D.E., Bekker, A., Miacchiarelli, R., Mazurier, A., Hammarlund, E.U., Boulvais, P., Dupuy, J.J., Fontaine, C., Füsi, F.T., Gauthier-Lafaye, F., Janvier, P., Javaux, E., Ossa-Ossa, F., Pierson-Wickmann, A.C., Riboulleau, A., Sardini, P., Vachard, D., Whitehouse, M., Meunier, A., 2010. Large colonial organisms with coordinated growth in oxygenated environments 2.1 billion years ago. Nature 466, 100–104.

El Albani, A., Bengston, S., Canfeld, D., Riboulleau, A., Rollion-Bard, C., Macchiarelli, R., Ngombi-Pemba, L., Hammarlund, E., Meunier, A., Mouele, I.M., Benzerara, K., Bernard, S., boulvais, P., Chaussidon, M., Cesari, C., fontaine, C., Chi-Fru, E., Ruiz, J.M.G., Gauthier-Lafaye, F., Mazurier, A., Pierson-Wickmann, A.-C., Rouxel, O., Trentesaux, A., Vecoli M., Versteegh, G.J.M., White, L., Whitehouse, M., Bekker, A., 2014. The 2.1 Ga Old Francevillian Biota: Biogenicity, Taphonomy and Biodiversity, PLOs One, 9, e99438.

Fritz P., Smith D.G.W., 1970. The isotopic composition of secondary dolomite. Geochim. Cosmochim. Acta 34, 1161-1173.

Gauthier-Lafaye, F., Weber, F., Ohmoto H., 1989. Natural fission reactors of Oklo. Econ. Geol. Bull. of the society of economic geologists 84, 2286-2295.

Gauthier-Lafaye, F., Weber, F. 1989. The Francevillian (Lower Proterozoic) uranium ore deposits of Gabon. Econ. Geol. 84, 2267–2285.

Gauthier-Lafaye, F., Weber, F., 2003. Natural nuclear fission reactors: time constraints for occurrence, and their relation to uranium and manganese deposits and to the evolution of the atmosphere. Precambrian Res. 120, 81–100.

Jaffrés, J.B.D., Shields, G.A., Wallmann, K., 2007. The oxygen isotope evolution of seawater: A critical review of a long-standing controversy and an improved geological water cycle model for the past 3.4 billion years. Earth Sci. Rev 83, 83-122.

Matthews, A., Katz, A., 1977. Oxygen isotope fractionation during the dolomitization of calcium carbonate. Geochim. Cosmochim. Acta 41, 1431–1438.

Ngombi-Pemba, L., El Albani, A., Meunier, A., Grauby, O., Gauthier-Lafaye, F., 2014. From detrital heritage to diagenetic transformations, the message of clay minerals contained within shales of the Palaeoproterozoic Francevillian basin (Gabon), Precam. Res. 255, 63-76.

Préat, A., Bouton, P., Thiéblemont, D., Prian, J.-P., Ndounze, S.S., Delpomdor, F., 2011. Paleoproterozoic high δ13C dolomites from the Lastoursville and Franceville basins (SE Gabon): Stratigraphic and synsedimentary subsidence implications. Precambrian. Res. 189, 212–228.

Taylor, S.R., McLennan, S.M., 1985. The Continental Crust: Its Composition and Evolution Blackwell, Oxford, 312p.

Vasconcelos, C., McKenzie, J.A., Warthmann, R., Bernasconi, S.M., 2005. Calibration of the $\delta^{18}O$ paleothermometer for dolomite precipitated in microbial cultures and natural environments. Geology 33, 317-320.

Weber, F., 1968. Une série précambrienne du Gabon: le Francevillien. Sédimentologie, Géochimie, relations avec les gites minéraux associés, Mem. Serv. Carte Geol. Alsace-Lorraine, Strasbourg 28, 32p.

Zheng, Y.F., 1999. Oxygen isotope fractionation in carbonate and sulfate minerals. Geochimical journal 33, 109-126.